New insights on the fossil arc of the Tyrrhenian Back-Arc Basin (Mediterranean Sea)

Published Version:
Palmiotto, C., Braga, R., Corda, L., Di Bella, L., Ferrante, V., Loreto, M.F., et al. (2022). New insights on the fossil arc of the Tyrrhenian Back-Arc Basin (Mediterranean Sea). TECTONOPHYSICS, 845, 1-14 [10.1016/j.tecto.2022.229640].

Availability:
This version is available at: https://hdl.handle.net/11585/903219 since: 2022-11-16

Published:
DOI: http://doi.org/10.1016/j.tecto.2022.229640

(Article begins on next page)

Palmiotto, Camilla; Braga, Roberto; Corda, Laura; Di Bella, Letizia; Ferrante, Valentina; Loreto, Maria Filomena; Muccini, Filippo: New insights on the fossil arc of the Tyrrhenian Back-Arc Basin (Mediterranean Sea)

TECTONOPHYSICS VOL. 845 ISSN: 0040-1951

DOI: 10.1016/j.tecto.2022.229640

New insights on the fossil arc of the Tyrrhenian Back-Arc Basin (Mediterranean Sea)

Camilla Palmiotto[a,*], Roberto Braga[b], Laura Corda[c], Letizia Di Bella[c], Valentina Ferrante[a], Maria Filomena Loreto[a], Filippo Muccini[d,e]

[a] *Consiglio Nazionale delle Ricerche, Istituto di Scienze Marine, via Gobetti 101, 40129, Bologna, Italy*

[b] *Dipartimento di Scienze Biologiche, Geologiche e Ambientali, Universita` di Bologna, Piazza di Porta San Donato 1, 40126, Bologna, Italy*

[c] *Dipartimento di Scienze della Terra, Universita` "La Sapienza", Piazzale Aldo Moro 5, 00185, Roma, Italy*

[d] *Istituto Nazionale di Geofisica e Vulcanologia, via di Vigna Murata 605, 00143, Roma, Italy*

[e] *Consiglio Nazionale delle Ricerche, Istituto di Geologia Ambientale e Geoingegneria, 00185 Roma, Italy*

[*] *Corresponding author*

Abstract

Geology, geophysics and geodynamics of the Tyrrhenian Back-Arc Basin (BAB; central Mediterranean Sea) have been studied extensively during the last 50 years. However, some topics are still open: for example, the possible migration of the volcanic arc during the Ionian subduction of the past few Ma. We improved our knowledge of the geodynamics of the Tyrrhenian BAB in the area South of the Vavilov Volcano by analyzing multibeam bathymetry and unpublished single-channel reflection seismic and magnetic data. Furthermore, we studied the petrology of igneous rocks as well as facies and microfaunas of carbonates dredged from the Aurelia and Augusto seamounts. The Aurelia basement is made of basalts with calc-alkaline affinity. Carbonates from the Aurelia and Augusto seamounts consist of cemented Mg-calcite biomicrite crusts rich in planktonic foraminifera not older than Early Pleistocene. Based on our results, we interpret the Augusto and Aurelia seamounts as part of the active volcanic arc seaward of the Tyrrhenian BAB in Late Pliocene–Early Pleistocene.

Keywords:

Back-Arc Basins Tyrrhenian Sea Volcanic Arcs Geodynamics Transfer Zones

Introduction

Back-Arc Basins (BABs) and volcanic arcs are two main features characterizing the upper plates along convergent plate boundaries (Uyeda and Kanamori, 1979; Leat and Larter, 2003). The relative kinematics, composition and thermal state of the upper and lower plates, together with the age of the subducting lithosphere and the morphotectonic inheritance of the upper plate, rule the extensional tectonics along the BABs and their progressive evolution from a younger rifting stage to a mature spreading stage (e.g., Parson and Wright, 1996; Fujiwara et al., 2001; Martinez and Taylor, 2002; Sdrolias and Muller, 2006; Weins et al., 2006; Schellart et al., 2007). BABs in a rifting stage do not show a BAB magmatism, as for example the Havre Trough in the Southern Pacific, characterized by an oblique southward propagating extension and by the absence of a clear spreading ridge (Caratori Tontini et al., 2019); mature BABs show a Back-Arc Spreading Center (BASC), i.e. the Mariana Spreading Center in the Pacific (Hynes and Mott, 1985), or the East Scotia Ridge in the Southern Atlantic (Livermore et al., 1997; Fretzdorff et al., 2002).

Here we focus on the Tyrrhenian Sea (located in the central Mediterranean Sea, between the Italian Peninsula and the Sardinia; Fig. 1), a peculiar case of BAB associated to compressional tectonics where the lower oceanic plate is subducting under continental lithosphere. The Tyrrhenian is a BAB formed by extensional tectonics due to the progressive eastward/south-estward retreat of the Ionian subduction (e.g., Malinverno and Ryan, 1986; Doglioni, 1991; Doglioni et al., 1999, 2004; Faccenna et al., 1997, 2001; Carminati et al., 1998; Sartori, 2003; Rosenbaum et al., 2008; Conti et al., 2017; Loreto et al., 2020). First studies on the regional geology and geodynamics of the Tyrrhenian were published during 1970s and 1980s (e.g., Barberi et al., 1973, 1978; Selli et al., 1977; Hsü et al., 1978; Wezel, 1982; Della Vedova et al., 1984; Sartori, 1986; Rehault et al., 1987; Trincardi and Zitellini, 1987; Savelli, 1988). An important contribution on the knowledge of the Tyrrhenian basin occurred with the Deep Sea Drilling Project (DSDP) Leg 42, the Ocean Drilling Program (ODP) Leg 107 (Kastens et al., 1988; Kastens and Mascle, 1990). A collection of multidisciplinary papers on the geology and geodynamics of the Tyrrhenian Sea was shown by Marani et al. (2004), after the deep seismic exploration of the central Mediterranean and Italy (CROsta Profonda project; Scrocca et al., 2003; Finetti, 2005) during the 1990s. Recently, seismic refraction data have been acquired during the MEDOC Cruises in the 2010 (Ranero et al., 2012) in order to display the velocity structure of the Tyrrhenian crust and uppermost mantle together with the Moho reflector geometry (Prada et al., 2014, 2016, 2018).

The Tyrrhenian Abyssal Plain (TAP), marked by the isobaths of the 3000 m in Fig. 1a, is floored by basaltic and ultramafic rocks covered by Pliocene-Quaternary sediments (Hsü et al., 1978; Kastens and Mascle, 1990). The TAP shows three huge fissural volcanoes (the Magnaghi, the Vavilov and the Marsili) located in the center of three different basins (Fig. 1a). The Marsili and the Aeolian Islands represent respectively the current magmatism in the back-arc basin and in the arc front (Fig. 1; Kastens et al., 1988; Kastens and Mascle, 1990; Faggion et al., 1999; Marani and Trua, 2002; Trua et al., 2002, 2018; Marani et al., 2004; Nicolosi et al., 2006; Rosenbaum et al., 2008; Cocchi et al., 2009; Ventura et al., 2013). The

Magnaghi and the Vavilov can be considered segments of extinct back-arc spreading centres evolved naturally in a basin characterized by frequent spreading jumps (Magni et al., 2021; Schliffke et al., 2022). In this paper we focus on the region East of the Magnaghi and South of the Vavilov volcanoes (Fig. 1a). This area shows an alternation of deep basins and high seamounts from which we have little understanding of their age and composition, given the lack of data. Some information can be extracted from studies of regional geology (Marani et al., 2004; Marani and Gamberi, 2004; Rovere and Wurtz, 2015; Palmiotto and Loreto, 2019; Pensa et al., 2019), the lithological and stratigraphic map of the Italian Seas (Colantoni et al., 1981), multichannel seismic reflection profiles (Finetti and Del Ben, 1986; Corradino et al., 2022) and the distribution of the regional magnetic data (Cella et al., 1998; Florio et al., 2022). In particular, we study two different seamounts (Aurelia and Augusto) in order to investigate their origin and to improve the geology and geodynamics of the central Tyrrhenian BAB.

We carried out a geophysical study based on: 1) multibeam bathymetry data downloaded from the European Marine Observation and Data Network (EMODnet; http://doi.org/10.12770/c7b53704-999d-4721-b1a3-4ec60c87238); 2) single-channel reflection seismics collected by the Institute of Marine Sciences (ISMAR) of the National Research Council (CNR) of Bologna in the 1970s (Fabbri et al., 1981; see Fig. 1a and methods); 3) magnetic data collected by the Institute of Marine Sciences (ISMAR) of the National Research Council (CNR) of Bologna in the 1990s (Bortoluzzi et al., 1999; see Fig. 1b and methods). We created regional bathymetry maps and an updated map of the reduced to pole magnetic anomalies of the central / Southern Tyrrhenian using magnetic data. Furthermore, we analyzed for the first time the petrology of igneous rocks and re-analyzed facies and microfauna of carbonates dredged at two seamounts South of the Vavilov Volcano. Results reveal new insights on the geodynamics of the Tyrrhenian BAB during the Late Pliocene-Early Pleistocene.

Material and methods

Bathymetry

Middle resolution bathymetric data (200 m-cell grid size) used in this paper have been downloaded from the European Marine Observation and Data Network (EMODnet; http://doi.org/10.12770/c7b537 04-999d-4721-b1a3-4ec60c87238). Spatial analysis and mapping of ASCII data used the open source software GMT (Wessel and Smith, 1998) with the nearest neighbour algorithm. Datum and projection used are, respectively, WGS84 and World Mercator. The Global Mapper Software has been used to create 2D digital elevation images.

Magnetic data

Magnetic data were collected by the CNR-ISMAR during the TIR-96 cruise onboard the R/V Gelendzhik in the 1996 and the TIR-99 cruise onboard the R/V A.N. Strakhov in the 1999 (Bortoluzzi et al., 1999). In total, >25,000 magnetic measurements along 1400 km of lines NNESSW oriented were used to create a new regional map (Fig. 1b). Raw data were corrected for spikes and diurnal variations using the reference station of L'Aquila (Central Italy). Magnetic anomalies were calculated by subtracting the IGRF (International Geomagnetic Reference field) model and then reducing the data to the North Pole by phase shifting them using the regional inclination and declination values of the IGRF.

Seismics

Seismic profiles used in this paper are part of an old large (about 46,000 km) dataset, available as profiles printed on paper, collected during several cruises carried out by CNR-ISMAR of Bologna between the 1970s and the 1980s (Fabbri et al., 1981). Seismic data have been shot using a Sparker 30 KJ and recorded with a trace length of 8 s (TWT). A new digital seismic database is under construction at the CNR-ISMAR of Bologna in order to preserve these data, inspired by FAIR (findable, accessible, interoperable and reusable) principles (Wilkinson et al., 2016). Seismic lines were scanned from paper to high resolution raster image (TIFF); they will then be converted into georeferenced SEG-Y format using the free Matlab program IMAGE2SEGY (Farran, 2008) distributed by the Department of Marine Geosciences of the Spanish National Research Council (http://www.icm.csic.es/gma/en/content/ image2segy/).

Here we present parts of five profiles acquired during oceanographic cruises T71, T73 and T75 (yellow, green and pink lines respectively and shown in Fig. 1a) onboard of the R/V Bannock carried out by the “Bacini Sedimentari” Group on behalf of the “Progetto Finalizzato Oceanografia e Fondi Marini” of the Italian CNR in the Tyrrhenian Basin (Fabbri et al., 1981).

Samples

Analyzed rocks were dredged by the CNR-ISMAR of Bologna during cruise T75 in the Tyrrhenian Sea. Samples labels refer to cruise, dredge station and rock samples numbers; for example, 75–30-3 refers to rock sample number 3, dredge station 30, carried out during the oceanographic expedition T75.

Samples dredged from site 75–30 (orange dot in Fig. 2a) are carbonates and volcanic rocks: volcanic samples have been re-analyzed; carbonates have been analyzed for the first time.

Samples dredged from sites 75–35 (yellow dot in Fig. 2a) and 75–36 (green dot in Fig. 2a), composed only of limestones, have been re-analyzed in order to determine the micropaleontological identifications and carbonate facies. Results of past samples analysis are shown in the lithological and stratigraphic map of the Italian Seas (Colantoni et al., 1981).

Rock samples underwent macroscopic and thin section examination under the petrographic and binocular microscopes. Bulk-rock abundances of major and minor elements were determined by X-ray fluorescence (XRF). Micropaleontological identifications were based on a bio and chronostratigraphical scheme for the Mediterranean of Iaccarino et al. (2007). Digital photographs and Energy Dispersive Spectroscopy (EDS) for elemental composition were obtained with a scanning electron microscope (FEI QUANTA 400) at the SEM Laboratory of Earth Sciences Department – Sapienza University of Rome (Italy). For the identification of crystalline material X-ray diffraction on sample powder were also carried out by a Phillips PANalytical X'Pert PRO diffractometer using CuKa radiation (n = 1.5418 Å), operating at 40 kV and 40 mA at a step size of 0.0260◦ at the Department of Earth Science, Sapienza University of Rome (Italy). The program used for qualitative analyses is WinPLOTR Programme (CDIFX UMR6226 Rennes/ILL Grenoble).

Results

Geophysics

Bathymetry and the reduced to the pole magnetic anomalies of the Southern Vavilov region maps are shown in Fig. 2. Part of sparker profiles here interpreted, with their values of magnetic anomalies associated, are shown in Fig. 3. Based on Loreto et al. (2020), three main seismic units have been identified: 1) a well-stratified unit (green color in Figs. 3 and 6), interpreted as Pliocene-Quaternary (PQ) deposits, based on lithostratigraphic information (Kastens et al., 1988); 2) a poorly-stratified and transparent unit (violet in color in Figs. 3 and 6), interpreted as coexisting sediments and volcanic layers; 3) a more chaotic and less reflective unit, interpreted as the basement (brown color in Figs. 3 and 6). Because of the low resolution of the Sparker profiles and their smaller size in Fig. 3, we created supplementary figures in order to zoom them and increase their resolution.

The Seamounts D'Ancona I and II, Plinia, Vavilov and Tibullo are located in the Northern part of the region, from West to East (Fig. 2). The D'Ancona is formed by two different seamounts located in the Eastern Magnaghi Abyssal Plain (EMAP; Fig. 2a). The D'Ancona I, a NNW-SSE oriented ridge, is located between 3485 m and 2696 m of depth; it is 19 km long and 12 km wide, with a steep western flank (20◦) and an eastern flank 10◦ steep (Fig. 2b). The D'Ancona II is a 13 km long and 11 km wide seamount, E-W oriented, with a depth ranges from 3476 m to 2900 m (Fig. 2a). The northern flank is 12◦ steep; the southern is 7◦ (Fig. 2b). From a magnetic viewpoint, the D'Ancona I shows a negative magnetic anomaly (from 0 to -50 nT), whereas the D'Ancona II a positive magnetic anomaly (> 100 nT). East of the D'Ancona II, there is a NNE-SSW oriented topographic ridge 17 km long and 6.5 km wide; it is unnamed in literature and here we called it "Plinia". This seamount ranges between 3150 m and 2647 m of depth (Fig. 2a), and it is characterized by a western flank steeper than the eastern side (20◦ and 15◦ respectively; Fig. 2b); the magnetic anomaly is negative and it ranges from 0 to -150 nT. The Southern part of the Plinia can be shown in the in the PM3E sparker profile of Fig. 3 (Box A and A') and Supp. Fig. 1, between the Fix 26 and 28, covered by a thin PQ unit. Plinia is located near Vavilov: they show a similar trend and value of magnetic anomaly (Fig. 2).

The Vavilov Seamount is located east of the Plinia Seamount. This huge submarine volcano rises from the abyssal plain at a depth of 3500 and arrives at only 793 m below sea level. The Vavilov shows an asymmetric perpendicular profile, with the western flank steeper than the eastern side (23◦ and 14◦ respectively; see the slope shader map of Fig. 2b). The depth of the volcano ranges from 3600 m to 823 m. The Vavilov shows a very strong negative magnetic anomaly (from 0 to -681 nT), although a small portion of its eastern flank shows a positive anomaly (from 0 to 150 nT). To the east of Vavilov, there is Tibullo Seamount, an elongated narrow NNE-SSW ridge, only 400 m high, characterized by a symmetric profile (flanks ~13◦ steep); the magnetic anomaly is positive (between 0 and 50 nT) on the northern part, and negative on the southern part (between 0 and 50 nT).

The Southern Vavilov Abyssal Plain (SVAP; mean depth ~ 3600 m) is filled by >500 m of sediments (PQ unit along the PM3E profile; Fig. 3 and Supp. Fig. 1). East of the SVAP, there is a seamount unnamed in literature, here called “Aurelia” (Fig. 2). The Aurelia is a WNW/ESEoriented seamount between 3500 m and 2750 m deep, characterized by a strongly asymmetrical perpendicular profile, with the northern flank steeper than the southern flank (25◦ and 12◦ respectively; Fig. 2b). The magnetic anomaly ranges from 0 to 50 nT in the western part and from 0 to -50 nT in the eastern part of this seamount. The profile PM4 (Fig. 3, Box B and B′ and Supp. Fig. 2) crosses perpendicularly the Aurelia, showing between Fix 75 and 76 a sub-vertical discontinuity that connects laterally the basement with the PQ unit. The Aurelia is crossed also by Profile PM11 (Fig. 3, Box C and C′ and Supp. Fig. 3): also here the asymmetry of the seamount, with a sub-vertical fault affecting the northern flank, is clearly visible. South of the Aurelia, the NNE-SSW oriented ridge Virgilio is formed by two different highs: the northern high (~ 2800 m of depth) with a shallow negative magnetic anomaly (from 0 to -50 nT); in contrast, the southern high (~ 2700 m of depth) with very strong positive values (> 100 nT).

The southern part of this region is characterized by two arc-shaped seamounts. One of those, the Augusto, a ~ 55 km-long seamount ranging from 3100 m to 1950 m of depth (Fig. 2a), is characterized by six peaks located between 2400 and 1950 m of depth (Fig. 2b). It shows a very strong positive magnetic anomaly, particularly in its central part (> 200 nT). The Augusto is separated from an unnamed seamount, here we call “Emilia” (minor depth 2200 m) from a NNW-SSE oriented basin. West of the Emilia, we have a deep (> -3500 m) and almost circular basin.

The NNE-SSW segment of the PM11 profile (Fig. 3, Box C and C′ and Supp. Fig. 3) crosses the Aurelia, a small basin filled by PQ sediments and Augusto. PQ sediments in the small basins are well-stratified and undeformed in the shallow part, while gently deformed in the deeper part. This intra-Pliocene unconformity corresponding probably to the “X Unconformity” (Zitellini et al., 1986) is marked with a violet horizon. Several NEand SWdipping normal faults control the formation of small basins (see at Fix 13 and 2 in the box C′ of Fig. 3).

The SW-NE oriented segment of the profile PM10E (Fig. 3, Box D and D′ and Supp. Fig. 4) crosses the Emilia, Augusto and Virgilio Seamounts. Emilia and Virgilio are bounded by several SWand NE-dipping normal faults, as suggested by the abrupt lateral interruption and dislocation of well-stratified PQ unit (marked in green). These normal faults dislocate also the basement and an intermediate unit (VIOLET) with a transitional seismo-stratigraphic character. The PQ unit covers part of these two seamounts, part of the intermediate unit and forms thick and narrow basins (see at Fix 17 of box D′ in Fig. 3). The Augusto seamount, with a chaotic seismo-stratigraphic character, does not show any sedimentary cover nor faults dislocations.

Facies and microfaunal associations

The sample dredged from site 75–30-3 (Aurelia Seamount; Fig. 2a) shows the direct contact between a few centimeters thick completely lithified limestone, and a greenish volcanic rock (Fig. 4a). The upper surface of the volcanic rock appears to be irregular and affected by frequent fractures filled by carbonate mud. A thin non-continuous brownish-to-black film marks the contact magmatic rock/limestone and locally also the neptunian-dykes walls. The carbonate crust overlying the volcanic rock appears to be completely lithified; its upper surface, exposed to seawater, is coated by a thin black film and is strongly colonized by serpulids that are, in turn, covered by a black film. Frequent microhollows representing the moulds of eroded and/or dissolved tests are recognizable.

Samples dredged from sites 75–35-(5–7-9) and 75–36-7 (Augusto Seamount; Fig. 2a) consist of 2–3 cm of light brownish consolidated limestones. No direct contact with volcanic rocks has been observed here. The limestone upper surface is coated by a black film strongly colonized by serpulids, which are in turn mineralized. In site 75–35 the carbonate crust is totally colonized by corals and serpulids. Most of the recovered corals are solitary cold-water species as Desmophyllum with characteristic cup-shaped morphology and marked septa (Fig. 4b). Their size varies from a few up to 6–7 cm; the younger individuals, growing on top of the older ones, simulate pseudo-colonies. The corals represent fossil occurrences; no living corals have been recovered. The corals surface appears to be almost completely covered by a very thin film, black in color.

All the carbonates consist of crusts cemented throughout their total thickness without textural evolution from chalk to limestones. Just in one sample (75–36-7a) a small cavity is filled by a not completely lithified planktonic-rich mud.

Microfaunal analysis of the carbonate crusts reveals coral fragments, gasteropods, pteropods, sponge spicules and foraminifera. The foraminiferal content is represented by planktonic taxa widely distributed in the hazel-brown micritic carbonate with mudstone texture or gathered inside bioturbation pockets, bioerosive structures and neptunian dykes within the volcanic substratum. Mn-Fe-oxides films (or permeation or crusts) always outline the bioerosion structures. The most frequent taxa are: Pulleniatina obliquiloculata, Globorotalia inflata, Globorotalia scitula, Orbulina universa and globigerinids (e.g. G. bulloides). Genus Globigerinoides is less abundant and it is mainly represented by G. trilobus. Globorotalia truncatulinoides (in the 75–30-3) and of Pulleniatina obliquiloculata were also observed (Fig. 4d).

X-ray diffraction on the carbonate crusts showed Mg-calcite and calcite as the most abundant phases with a subordinate silicate fraction with mica, chlorite, quartz, and probably montmorillonite. Also SEM analysis, coupled with EDS, showed predominance of carbonate composition with a very subordinate clay-sized silicate fraction (Fig. 4a). Isolated volcanic minerals (quartz and feldspar) and volcanic fragments have been found within the carbonate crust from site 75–36-7 (Fig. 4c).

The thin brownish-to-black film marking the contact magmatic rock/ limestone and the neptunian-dykes walls is of Mn–Fe oxides (Fig. 4a) and shows a thin layered structure. All limestone surfaces, borings (Fig. 4e) and/or skeletons exposed to sea-water are coated by a Mn and Fe-oxy-hydroxides thin black-brownish botryoidal film with a laminated texture. The major mineral phase is todorokite, with subordinate amounts of phosphates and montmorillonite (X-ray diffraction data).

Based on thin section and SEM-EDS observations, the limestones exhibit a complex diagenetic history. Sometimes the carbonate crusts are characterized by a first thin portion of an early consolidated limestone with bioclastic fragments and diffuse serpulids separated, by means of a thin film of Mn-Fe-oxides, from a portion richer in planktonic foraminifera. The lower portion may display borings and/or fractures, coated by a Mn–Fe oxides film, filled by carbonate pelagic sediments that, in turn underwent a new early lithification and mineralization. All these features indicate at least two phases of early diagenesis accompanied by Mn–Fe mineralization. Both the mineralogical composition and the planktonic associations of the two portions do not show significant differences.

Petrography

Samples were chosen for petrographic analyses to verify or discard their igneous nature. In particular, we selected samples with phyric-like texture, i.e. large minerals in an aphanitic ground mass. Sample T75–303 (Aurelia Seamount; Fig. 2a) shows white to light-brown grains up to two mm across set in a gray-greenish matrix (Fig. 5a1). A vein of 10 mm maximum apparent thickness cuts the sample. The vein is filled by very fine-grained material and the contact with the host rock is sharp. Sample T75–30-5 displays phyric texture made of vitreous grains (average 1 mm across) in a relatively soft light-gray matrix (Fig. 5a2). Inspection under a polarizing optical microscope (Fig. 5a3,4) reveals a texture with euhedral to anhedral grains set in a chlorite and opaque-rich matrix. Matrix minerals are locally aligned to form a fluidal texture. Two types of grains are recognized: (1) euhedral to subhedral grains with pseudohexagonal and prismatic shapes (Fig. 5a4,5) and (2) rounded fractured grains with clear appearance under plane polarized light (Fig. 5a3). The euhedral to subhedral grains may be former phenocrysts now completely replaced by secondary chlorite and carbonates, mainly dolomite and minor Mg-calcite, as determined by energy-dispersive spectrometry in a SEM. These phenocrysts occur as single grains or as clusters that locally gives the rock a glomeroporphyritic texture. The rounded fractured grains are made of quartz (sample T75–30-3). The matrix is composed of euhedral to subhedral microlites, now completely replaced by secondary low-Fe chlorite, and rounded Ti-rich minerals. High-Fe chlorite fills the interstices among microlites. Sample T75–30-5 is cut by at least two sets of veins. Earlier veins, maximum thickness 0.25 mm, are filled by coarse grained Fe-bearing dolomite with irregular shapes. Late veins are wider, and are filled by euhedral dolomite. Finally, sample T75–30-5 contains amygdale showing a zonation, from rim to core of the amygdala, chlorite, opaque material and dolomite (Fig. 5a6).

Discussion

Environmental significance of the Aurelia and Augusto rocks and carbonate facies

Samples of rock analyzed from the Aurelia seamount preserve a porphyritic texture with different types of phenocrysts set in a matrix with microlites that locally define a flow texture. These features are compatible with an igneous nature of the samples. Their primary mineralogy is now replaced by secondary phases such as low-Fe chlorite and dolomite. Similarly, the matrix contains microlites now replaced mainly by low-Fe chlorite, and Ti-rich phases that possibly represent remnants of primary Fe–Ti oxides that underwent iron loss during lowtemperature rock-water interaction. Plotting our data of Ti and Zr, two elements usually interpreted as relatively immobile during low-T alteration (Pearce, 2014), the rocks of the Aurelia Seamount fall in the calc-alkaline field (Fig. 5b).

From a carbonate/biostratigraphic viewpoint, samples from the Aurelia and Augusto

Seamounts consist of crusts cemented throughout their total thickness without textural evolution from chalk to limestones. The crusts, with thickness between 15 and 30 mm, are made of Mgcalcite biomicrite rich in planktonic foraminifera with a very subordinate silicate component. The occurrence of Globorotalia truncatulinoides on the Aurelia Seamount suggests for this sample an age not older than Early Pleistocene (Iaccarino et al., 2007). This is also confirmed by the presence of Pulleniatina obliquiloculata, a warm tropical-subtropical species, that although it occurred in the Atlantic basin in Early Pliocene (Zankl, 1969; Bolli and Saunders, 1985; Iaccarino et al., 2007), it is never recorded in Pliocene Mediterranean deposits. Moreover, according to Bolli and Saunders (1985), P. obliquiloculata shows major frequency peaks during the Pleistocene–Holocene time interval. This taxon would have entered the Mediterranean during the Pleistocene warmer climatic stages (Conti et al., 2013) probably from the Atlantic occurring exclusively in the western sector of the Mediterranean basin. An interesting feature is the occurrence within the carbonate crust from the Augusto Seamount of isolated volcanic minerals (quartz and feldspar) and of volcanic fragments, probably indicating a coeval magmatic activity or alternatively a supply of volcanic material eroded from a nearby seamount.

The occurrence in many areas of the Mediterranean of Quaternary deep-water cemented limestones with different grades of consolidation, from brittle to consolidated chalk to cemented limestones, has been reported in literature (Allouc, 1990). The study of the carbonate crusts and their relationships with the volcanic substrate, are important for understanding the rapid formation of hardgrounds in ancient sedimentary sequences.

A number of studies have focused on the driving mechanisms for the early lithification of the Quaternary deep-sea crusts (Emelyanov and Shimkus, 1986; McKenzie and Bernoulli, 1982; Allouc, 1987, 1990; Remia et al., 2004). Early lithification, occurring at or below the seafloor, takes place under varying conditions: it may occur in sedimentstarved environments, it may depend on ascending interstitial carbonate-rich waters, or on microbiological precipitation or it may be physiochemically controlled and related to inward diffusion of seawater solutions. Concerning the degree of saturation relative to calcite, Mediterranean waters remained saturated at all depths also during the Pleistocene cold phases (Allouc, 1987). Another significant factor controlling carbonate precipitation or dissolution is the concentration of dissolved phosphates and organic matter (Morse, 1986). The carbonate crusts taken into consideration in this study are predominantly made of Mg-calcite with a very subordinate silicate fraction, mostly represented by mica, quartz chlorite and montmorillonite, probably deriving from the weathered volcanic substrate. One of the factors controlling early lithification is the purity of lime mud; <2% of insoluble residue (especially clay minerals) favors cementation and recrystallization (Zankl, 1969).

Nevertheless an excess of hydrothermal metals (i.e. Mn-Fe-oxyhydroxides) may “fertilize” areas of normal biological productivity, resulting in massive phytoplankton blooms (Coale et al., 1996; Larson and Erba, 1999; Corda and Palmiotto, 2015). The microorganisms activity may have a significant influence in precipitating hydrothermal Mn-Fe-oxyhydroxide (Dekov and Savelli, 2004); in addition, Mutti and Bernoulli (2003) stress the relationship between phosphate mineralization, trophic resources and microbial micrite precipitation. Based on our observations, we assume a significant role of the microbiological precipitation of calcite in facilitating the early lithification of planktonic ooze.

Sources of magnesium are usually seawater and sometimes, fresh waters but could also derive from weathered magmatic Fe–Mg rich rocks. When magnesium is delivered to seawater, Mg-calcite can precipitate (Mackenzie and Andersson, 2013; Morse and McKenzie, 1990).

The limited thickness of the carbonate crusts points to very slow rates of sedimentation and/or accumulation probably related to high hydrodynamics. The very thin brownish film of Mn–Fe oxides, even if noncontinuous, covering the volcanic substrate hints at a period of waterrock exposure before the carbonate planktonic-rich mud began to deposit. During this period the volcanic substrate underwent a phase of extensional tectonics promoting intense fracturing, as testified by neptunian dykes partially mineralized and successively filled by pelagic sediments. This substrate should be firstly colonized by small rapidlygrowing opportunistic organisms such as serpulids, favored by strong storm activity, and covered by few millimeters of carbonate mud cemented early. Above this first phase of sedimentation, accompanied by early diagenesis, bioturbation processes and Mn–Fe mineralization, a new phase of sedimentation of carbonate planktonic-rich ooze began, that was rapidly lithified and mineralized.

Ultimately our findings suggest that the pelagic sediments settled on the magmatic substrates underwent an early lithification process induced by precipitation of Mg-calcite within the pelagic carbonate matrix in areas of very slow sedimentation rates. The volcanic substrates underwent a tectonic instability, testified by fractures and neptunian dykes infilled by planktonic mudstones. Their morphostructural configuration as isolated highs, suffering high hydrodynamic conditions, is here interpreted as responsible for low sedimentation/accumulation rates, clustering of planktonic foraminifera and skeletal fragmentation. The slow rates of deposition favored prolonged conditions of exposure at the seawater-sediment interface of the pelagic and skeletal carbonates, enhancing the diffusion of seawater-ions throughout the sediments and promoting chemical precipitation and the consequent development of hardgrounds prone to be colonized by corals and serpulids. In addition, the presence of phosphorous as evidenced by the SEM-EDS analysis, suggests that the pelagic carbonates underwent early diagenetic lithification phases under high-fertility conditions which, favoring an increase of microbiota communities, promoted an increase of microbiological micrite precipitation. The widespread Mn–Fe mineralizations covering both the carbonate deposits and the encrusting/colonizing biota on the base of crust morphologies, textural evidence and tectonic setting, can be related to hydrothermal processes.

Geodynamic significance of the Aurelia and Augusto seamounts

We discuss here the significance of the Aurelia and Augusto seamounts in the geodynamics of the central Tyrrhenian BAB, based on our results, on data from literature, on the regional bathymetry map and the map of the distribution of the reduced to the pole magnetic anomalies of the Southern Tyrrhenian (Fig. 6a and b, respectively).

The Magnaghi Basin (Fig. 6a) starts opening during the Tortonian/ Messinian (Loreto et al., 2020). Volcanism of the Magnaghi Volcano ischaracterized by basalts with an Na-alkaline affinity, dated from 3.1 to2.7 Ma (Late Pliocene; Serri et al., 2001), in line with the subchron C2An.1n (3.040 to 2.581 Ma; Cande and Kent, 1995) shown in Fig. 6b. The Vavilov Basin (Fig. 6a) opened between the Late Miocene and the Early Pliocene (the older basalts from the ODP 373 are 7.5 Ma old; Hsü et al., 1978) when their composition is similar to mid-ocean ridges (MORB), as shown by the basalts sampled from the ODP 655 on the Gortani Ridge (Fig. 6a), dated ~4 Ma (Kastens et al., 1988). The beginning of the Vavilov Volcano activity is placed at 3 Ma, at the same time of the spreading of the basin (Robin et al., 1987). The Vavilov lavas, very similar to those of the Magnaghi Volcano, are formed by basalts ranging from tholeiitic to Na-alkaline (Peccerillo, 2017). The end of extension in the Vavilov Basin allows the growth of the volcano, which shows in Fig. 6b a negative magnetic anomaly (C2r.2r; 2.581 to 2.150 Ma; Savelli and Ligi, 2017). According to Parson et al. (1990), the change in chemical composition from MORB to calc-alkaline marks the evolution of a back-arc basin from an early stage, where a pure extensional tectonics produced an oceanic crust with MORB affinity, to a mature stage of back arc spreading, where the oceanic crust has a calc-alkaline affinity. Based on the age of the boundary between the older sediments and calc-alkaline rocks sampled in the ODP 651 (Northern Vavilov Basin; Kastens et al., 1988; Bonatti et al., 1990), we assume that the extensional tectonics of the Vavilov Plain continued until 2.6 Ma.

The Marsili Basin (Fig. 6a) starts opening in the Early Pleistocene (basalts dated ~2 Ma from the OPD 650; Kastens et al., 1988); it shows a negative/inverse magnetic anomaly falling in the chron C1r.2r (1.770 to 1.070 Ma; Fig. 6b). The Marsili Volcano is located in the center of the basin, formed by calc-alkaline rocks (Trua et al., 2002) not older than 1.07 Ma (Cocchi et al., 2009), corresponding with the positive/normal magnetic anomaly C1n (0.780 to 0.00 Ma; Cocchi et al., 2009; see Fig. 6b). The Marsili is surrounded by several volcanic islands and seamounts (Fig. 6a): the Palinuro Volcanic Complex, a E-W oriented volcanic structure formed by basaltic-andesite compositions lavas dated 0.8–0.3 Ma (e.g., Colantoni et al., 1981; Cocchi et al., 2017); the Alcione, and Lametini 1 and 2 seamounts, related to the geodynamic environment to the Aeolian arc and younger than 1 Ma (Barberi et al., 1973; Beccaluva et al., 1985; Lupton et al., 2011); the Aeolian Islands, consisting of calc-alkaline to shoshonitic lavas and pyro-clastics, with minor potassic alkaline rocks (Peccerillo, 2005), originated by volcanism due to the "wet" melting of a suprasubduction mantle wedge (Lupton et al., 2011); the Enarete, Eolo, Sisifo and Tiro seamounts, the oldest volcanoes of the Aeolian Islands Arc (Beccaluva et al., 1982, 1985). All these volcanoes and seamounts show a normal/positive magnetic anomaly (i. e. Bortoluzzi et al., 2010; Cocchi et al., 2017) that, as in Marsili, can be attributed to the C1n (0.780 to 0.00 Ma), although some of them show a volcanism >0.780 Ma, before the formation of the Marsili Volcano. For example, the Tiro and Sisifo seamounts are formed by calc-alkaline and high K2O calcalkaline rocks dated ~1.5 Ma and from 1.3 Ma to 0.9, respectively (Beccaluva et al., 1985); Enarete and Eolo, formed by basalts, dacites and rhyolites, have been dated between 0.85 and 0.77 Ma (Beccaluva et al., 1982, 1985; Trua et al., 2004).

Based on the geodynamic models of Carminati et al. (2010), we reconstructed a cartoon showing the migration of the volcanic arc associated to the Ionian slab during the last 3 Ma (Fig. 7). In this cartoon, at 3 Ma, when the Magnaghi and Vavilov volcanoes were active, we assume that Aurelia, Virgilio and the western part of Augusto were part of the active volcanic arc. We based on: 1) the calc-alcaline basement rocks of the Aurelia (Ti/Z diagram data of Fig. 5b), indicating a subduction-related volcanism; 2) the calc-alcaline basement rocks of the western part of the Augusto (Colantoni et al., 1981), testified also by the occurrence of volcanic fragments in our carbonate samples, and on the strong positive magnetic anomaly (Fig. 6b and Cella et al., 1998); 3) the volcanic nature of the Virgilio, considered a NNE-SSW oriented composite volcanic structure made by a coalescence of a series of centres (Finetti and Del Ben, 1986); 4) the recognized planktonic foraminifera assemblages of the Aurelia and Augusto carbonates, cannot be older than Early Pleistocene, indicating a volcanic activity before 2.58 Ma.

Based on the bathymetry maps (Figs. 2 and 6a), the Augusto seamount is composed by several peaks forming a curved arc, located between 2400 and 1900 m below sea level. This curved morphology resembles more the fossil Aeolian volcanic arc, South of the Marsili, formed by the seamounts Sisifo and Tiro, active between 1.5 and 1 Ma (Fig. 7 1 Ma; Beccaluva et al., 1985), than the morphology of the modern Aeolian volcanic arc (Fig. 7–0 Ma). Considering the location of the Augusto, between the Aurelia and the Augusto, and the Sisifo and Tiro, and based on the age of their volcanism, we assume the Augusto as part of the Early/Middle Pleistocene Tyrrhenian volcanic arc (Fig. 7 2 Ma). The different trend of the Tyrrhenian volcanic arc between the Late Pliocene (Fig. 7 3 Ma) and the Early Pleistocene (Fig. 7 – from 2 to 0 Ma) could testify the change from eastward to southeastward of the Ionian slab retreat, due to collision with the Apulia platform to the north and the Hyblean platform to the south, during the Pliocene (Van Van Dijk et al., 2000). The geodynamic model by Corradino et al. (2022) considers the area between Vavilov and Marsili as the present place of back-arc extension, and the Marsili as part of a Pliocene volcanic arc. In contrast, our geological, geochronological and petrological results show that the seamounts Aurelia and Augusto were part of the active Tyrrhenian volcanic arc during the Late Pliocene-Early Pleistocene, and that the Marsili is the present back-arc spreading center (positive/normal magnetic anomaly C1n 0.780 to 0.00 Ma; Fig. 6b).

The Vavilov-Marsili transfer zone

According to Macdonald et al. (1988) and Pagli et al. (2019), along the BABs, seafloor spreading is offset by transfer zones where strike-slip tectonics transfers displacement between two similar non-coplanar structures. Transfer zones are striking parallel to the regional direction of extension. They are local and passive fracture formed in response to active faulting on faults which link with the transfer; an example is transfer zone is the Central Lau Spreading Centre (CLSC) and the Eastern Lau Spreading Centre (ELSC) in the Lau Back-arc Basin (SW Pacific Ocean; Parson and Wright, 1996). Also, transfer zones could also be inherited from the overriding plate, as in the Northern Lau Basin, where the upper plate is affected by strike-slip tectonics along older tectonic lineaments (Palmiotto et al., 2022).

The central region of the Tyrrhenian BAB is characterized by a WNWESE oriented basin, located between the Vavilov and the Marsili basins, perpendicular to the NNE-SSW trend of the Vavilov and Marsili volcanoes (Fig. 6a). This basin shows low values of magnetic anomalies (Fig. 6b) and, based on seismic refraction data (Recq et al., 1984), it is characterized by a minimum value of crustal thickness (the velocity is 6 km/s at only 5 km of depth). We show here part of a sparker profile (PM12; Fig. 6c and Supp. Fig. 5), acquired during the oceanographic expedition T71 (see the Fig. 1a and the methods). The profile PM12 is NE-SW oriented and crosses perpendicular the basin between Vavilov and Marsili. An interpretation of the profile shows that the basin is covered by PQ sediments and it shows in its center, from fix 32 to 37 (Fig. 6c and Supp. Fig. 5), a feature we interpreted as a positive flower structure. This feature can be attributed to a transcurrent fault that in the bathymetry map (Fig. 6a) can be followed from the Southern Vavilov Basin, where affects the Aurelia basement (see the sub-vertical fault in the profiles PM4 and PM11 of Fig. 3 and Supp. Figs.3,4), to the Western Marsili Basin. Furthermore, based on the maps of the distribution of the reduced to the pole magnetic anomalies (Figs. 2c,d and 6b), the upper part of the Vavilov Volcano and a small part of its eastern flank show a positive magnetic anomaly which could be attributed to a recent volcanic event, considering that the summit lavas have been dated between 0.37 and 0.09 Ma (C1n; Robin et al., 1987; Savelli and Ligi, 2017). Based on those considerations, we interpreted the Tyrrhenian as a BAB where two different segment of spreadings are active at the same time and, the basin between the Vavilov and the Marsili, their “Transfer Zone” (Figs. 6 and 7).

Conclusions

We analyzed geophysical and geological data of two seamounts (Augusto and Aurelia) located South of the Vavilov Volcano. The Augusto is characterized by an arc-shaped morphology, with several peaks located between 1950 and 2400 m below sea level; the Aurelia shows an asymmetric perpendicular profile due sub-vertical faults affecting its northern side, visible both from bathymetry and from the sparker profiles. The distribution of the reduced to the pole magnetic anomalies shows positive values on the Augusto, and low negative values on the Aurelia. Samples of rocks dredges from the Aurelia and the Augusto show a magmatic nature of their basement (basalts with a calkalcaline affinity). Carbonate samples consist of thin crusts cemented early made of Mg-calcite biomicrite rich in planktonic foraminifera, dated not older than Early Pleistocene. Based on our results, we interpret the Augusto and Aurelia as part of the volcanic arc of the Tyrrhenian BAB during the Late Pliocene–Early Pleistocene time.

Acknowledgements

Work supported by the Italian National Research Council (Consiglio Nazionale delle Ricerche). We thank Enrico Bonatti for the revision of the English; Marco Ligi for constructive comments that helped us to improve the manuscript; Marzia Rovere and Maria

Filomena Loreto for starting the creation of a digital seismic database of the old Sparker data at the CNR-ISMAR of Bologna. We are also grateful to the Editor and to the Reviewers for their constructive comments that helped improve the manuscript.

References

Allouc, J., 1987. Les paléocommunautés profondes sur fond rocheuxdu Pléistocène méditerranéen. Description et essai d'interprétation paléoécologique. Geobios 20 (2), 241–263.

Allouc, J., 1990. Quaternary crusts on slopes of the Mediterranean Sea: a tentative explanation for their genesis. Mar. Geol. 94, 205–238.

Barberi, F., Gasparini, P., Innocenti, F., Villari, L., 1973. Volcanism of the southern Tyrrhenian Sea and its geodynamic implications. J. Geophys. Res. 78 (23), 5221–5232.

Barberi, F., Bizouard, H., Capaldi, G., Ferrara, G., Gasparini, P., Innocenti, F., Joron, J.L., Lambret, B., Treuil, M., Allegre, C., 1978. Age and nature of basalts from the Tyrrhenian Abyssal Plain. From Hsü, K., et al., 1978. Site 373: Tyrrhenian Basin. Initial reports of the Deep Sea Drilling Project, 42(part 1). U.S. Government Printing Office, Washington, D.C, pp. 151–174.

Beccaluva, L., Rossi, P.L., Serri, G., 1982. Neogene to recent volcanism of the southern Tyrrhenian-Sicilian area: Implications for the geodynamic evolution of the Calabrian arc. Earth Evol. Sci 3, 222–238.

Beccaluva, L., Gabbianelli, G., Lucchini, F., Rossi, P.L., Savelli, C., 1985. Petrology and K/Ar ages of volcanics dredged from the Eolian seamounts: implications for geodynamic evolution of the southern Tyrrhenian basin. Earth Planet. Sci. Lett. 74 (2–3), 187–208.

Bolli, H.M., Saunders, J.B., 1985. Oligocene to Holocene low latitude planktic foraminifera. In: Bolli, H.M., Saunders, J.B., Perch-Nilsen, K. (Eds.), Plankton Stratigraphy. Cambridge University Press, Cambridge, pp. 155–262.

Bonatti, E., Seyler, M., Channell, J., Giraudeau, J., Mascle, G., 1990. Peridotites drilled from the Tyrrhenian Sea, Odp Leg 1071. In: Kastens, K.A., Mascle, J., et al. (Eds.), Proceedings of the Ocean Drilling Program, Scientific Results, Vol. 107, College station, Texas.

Bortoluzzi, G., Carrara, G., Fabretti, P., Gamberi, F., Marani, M., Penitenti, D., Stanghellini, G., Tonani, M., Zitellini, N., Bonazzi, C., Lippolis, S., Musacchio, M., Daviddi, A., Diroma, G., Ferrarini, A., Leotta, A., Gilod, D., Nikaronenkov, B., Efimov, V., Erofeev, S., 1999. Swath bathymetry and geophysical survey of thetyrrhenian sea report on bathymetric, magnetic and gravimetric investigations during cruises tir96 and tir99. In: IGM TECHNICAL REPORT N. 52, Bologna. http://ricerca.ismar.cnr.it/CRUISE_REPORTS/1990-1999/GELENDZHIK_TIR96_99_REP.

Bortoluzzi, G., Ligi, M., Romagnoli, C., Cocchi, L., Casalbore, D., Sgroi, T., Cuffaro, M., Caratori Tontini, F., D'Oriano, F., Ferrante, V., Remia, A., Riminucci, F., 2010. Interactions between volcanism and tectonics in the western Aeolian sector, southern Tyrrhenian Sea. Geophys. J. Int. 183, 64–78.

Cande, S.C., Kent, D.V., 1995. Revised Calibration of the Geomagnetic Polarity Timescale for the late cretaceous and Cenozoic. J. Geophys. Res. Solid Earth 100, 6093–6095. Cann, J.R., 1970. Rb, Sr, Y, Zr and Nb in some ocean floor basaltic rocks. Earth Planet. Sci. Lett. 10, 7–11.

Caratori Tontini, F., Bassett, D., De Ronde, C.E.J., Timm, C., Wysoczanski, R., 2019. Early evolution of a young back-arc basin in the Havre Trough. Nat. Geosci. 12, 856–862.

Carminati, E., Wortel, M.J.R., Meijer, P.T., Sabadini, R., 1998. The two-stage opening of the western–Central Mediterranean basins: a forward modeling test to a new evolutionary model. Earth Planet. Sci. Lett. 160 (3–4), 667–679.

Carminati, E., Lustrino, M., Cuffaro, M., Doglioni, C., 2010. Tectonics, magmatism and geodynamics of Italy: What we know and what we imagine. In: Beltrando, M., Peccerillo, A., Mattei, M., Conticelli, S., Doglioni, C. (Eds.), The Geology of Italy, J. Virtual Explor (ISSN 1441–8142, Vol. 36).

Cella, F., Fedi, M., Florio, G., Rapolla, A., 1998. Boundaries of magnetic anomaly sources in the Tyrrhenian region. Ann. Geophys. 51 (1), 1–23.

Coale, K.H., Fitzwater, S.E., Gordon, R.M., Johnson, K.S., Barber, R.T., 1996. Control of community growth and export production by upwelled iron in the equatorial Pacific Ocean. Nature 379, 621–624.

Cocchi, L., Caratori Tontini, F., Muccini, F., Marani, M.P., Bortoluzzi, G., Carmisciano, C., 2009. Chronology of the transition from a spreading ridge to an accretional seamount in the Marsili backarc basin (Tyrrhenian Sea). Terra Nova 21, 369–374.

Cocchi, L., Passaro, S., Caratori Tontini, F., Ventura, G., 2017. Volcanism in slab tear faults is larger than in island-arcs and back-arcs. Nat. Commun. 8, 1451.

Colantoni, P., Fabbri, A., Gallignani, P., Sartori, R., Rehault, J.P., 1981. Carta Litologica e Stratigrafica dei Mari Italiani. Scale 1:500.000. Litografica Artistica Cartografica, Firenze.

Conti, A., Bigi, S., Cuffaro, M., Doglioni, C., Scrocca, D., Muccini, F., Cocchi, L., Ligi, M., Bortoluzzi, G., 2017. Transfer zones in an oblique back-arc basin setting: Insights from the Latium-Campania segmented margin (Tyrrhenian Sea). Tectonics 36 (1), 78–107.

Conti, M.A., Girasoli, D.E., Frezza, V., Conte, A.M., Martorelli, E., Matteucci, R., Chiocci, F.L., 2013. Repeated events of hardground formation and colonisation by endo-epilithozoans on the sediment-starved Pontine continental slope (Tyrrhenian Sea, Italy). Mar. Geol. 336, 184–197.

Corda, L., Palmiotto, C., 2015. Rhodalgal–foramol facies in equatorial carbonates: insights from Miocene tectonic islands of the Central Atlantic. Palaeogeogr. Palaeclimatol. Palaeoecol. 428, 21–30.

Corradino, M., Balasz, A., Faccenna, C., Pepe, F., 2022. Arc and forearc rifting in the Tyrrhenian subduction system. Sci. Rep. 12, 4728.

Dekov, V.M., Savelli, C., 2004. Hydrothermal activity in the SE Tyrrhenian Sea: an overview of 30 years of research. Mar. Geol. 204, 161–185.

Della Vedova, B., Pellis, G., Foucher, J.P., Rehault, J.-P., 1984. Geothermal structure of the Tyrrhenian Sea. Mar. Geol. 55, 271–289.

Doglioni, C., 1991. A proposal for the kinematic modelling of W-dipping subductions: possible applications to the Tyrrhenian-Apennines system. Terra Nova 3, 423–434.

Doglioni, C., Gueguen, E., Harabaglia, P., Mongelli, F., 1999. On the origin of W-directed subduction zones and applications to the western Mediterranean. Geol. Soc. Spec. Publ. 156, 541–561.

Doglioni, C., Innocenti, F., Morellato, C., Procaccianti, D., Scrocca, D., 2004. On the Tyrrhenian Sea opening. Mem. Descr. Carta Geol. d'It. 44, 147–164.

Emelyanov, E.M., Shimkus, K.M., 1986. Geochemistry and Sedimentology of the Mediterranean Sea. Sedimentology and Petroleum Geology, Reidel, Dordrecth, p. 553.

Fabbri, A., Gallignani, P., Zitellini, N., 1981. Geologic evolution of the peri-Tyrrhenian sedimentary basins. In: Wezel, F.C. (Ed.), Sedimentary Basins of Mediterranean Margins. C.R.N., Italian Project of Oceanography, Tecnoprint, Bologna, pp. 101–126.

Faccenna, C., Mattei, M., Funiciello, R., Jolivet, L., 1997. Styles of back-arc extension in the Central Mediterranean. Terra Nova 9 (3), 126–130.

Faccenna, C., Becker, T.W., Lucente, F.P., Jolivet, L., Rossetti, F., 2001. History of subduction and back arc extension in the Central Mediterranean. Geophys. J. Int. 145 (3), 809–820.

Faggion, O., Pinna, E., Savelli, C., Schreider, A.A., 1999. Geomagnetism and age study of Tyrrhenian Seamounts. Geophys. J. Int. 123, 915–930.

Farran, M., 2008. IMAGE2SEGY: Una aplicacion informatica para la conversion de imagenes de perfiles sísmicos a ficheros en formato SEG Y. Geo-Temas 10, 1215–1218.

Finetti, I.R., 2005. In: Finetti, I.R. (Ed.), CROP project: deep seismic exploration of the Central Mediterranean and Italy, vol. 1. Elsevier.

Finetti, I.R., Del Ben, A., 1986. Geophysical study of the Tyrrhenian opening. Boll. Geofis.

Teor. Appl. 28, 75–155.

Florio, G., Passaro, S., de Alteriis, G., Cella, F., 2022. Magnetic anomalies of the Tyrrhenian Sea revisited: a processing workflow for enhancing the resolution of aeromagnetic data. Geosciences 2022 (12), 377.

Fretzdorff, S., Livermore, R.A., Devey, C.W., Leat, P.T., Stoffers, P., 2002. Petrogenesis of back-Arc East Scotia Ridge, South Atlantic Ocean. J. Petrol. 43, 1435–1467.

Fujiwara, T., Yamazaki, T., Joshima, M., 2001. Bathymetry and magnetic anomalies in the Havre Trough and southern Lau Basin: from rifting to spreading in back-arc basins. Earth Planet. Sci. Rev. 185, 253–264.

Hsü, K., Montadert, L., Bernoulli, D., Bizon, G., Cita, M.B., Erickson, A., Fabrcius, F., Garrison, R.E., Kidd, R.B., M`eler´es, F., Müller, C., Wright, C.R., 1978. Site 373: Tyrrhenian Basin. Initial Reports of the Deep Sea Drilling Project 42(part 1). U.S. Government Printing Office, Washington, D.C, pp. 151–174.

Hynes, A., Mott, J., 1985. On the causes of back-arc spreading. Geology 13, 387–389.

Iaccarino, S., Premoli Silva, I., Biolzi, M., Foresi, L.M., Lirer, F., Turco, E., Petrizzo, M.R., 2007. Practical manual of Neogene Planktonic Foraminifera. International School on Planktonic Foraminifera, 6th course, Perugia 19-23 February 2007. University of Perugia, pp. 1–181.

Kastens, K., Mascle, J., Auroux, C., Bonatti, E., Broglia, C., Channell, J., Curzi, P., Emeis, K.-C., GlaçOn, G., Hasegawa, S., Hieke, W., Mascle, G., Mccoy, F., Mckenzie, J., Mendelson, J., MüLler, C., R´ehault, J.P., Robertson, A., Sartori, R., Sprovieri, R., Torii, M., 1988. ODP Leg 107 in the Tyrrhenian Sea: Insights into passive margin and back-arc basin evolution. Geol. Soc. Am. Bull. 100 (7), 1140–1156.

Kastens, K.A., Mascle, J., 1990. The geological evolution of the Tyrrhenian Sea: an introduction to the scientific results of ODP Leg 107. In: Kastens, K.A., Mascle, J., et al. (Eds.), Proceedings of the Ocean Drilling Program, Scientific Results, vol. 107. Ocean

Drilling Program, College station, Texas, pp. 3–26.

Larson, R.L., Erba, E., 1999. Onset of the mid-cretaceous greenhouse in the Barremian–Aptian: igneous events and the biological, sedimentary, and geochemical responses. Paleoceanography 14, 663–678.

Leat, P.T., Larter, R.D., 2003. Intra-oceanic subduction systems: introduction. Geol. Soc. Lond., Spec. Publ. 219, 1–17.

Livermore, R., Cunningham, A., Vanneste, L., Larter, R., 1997. Subduction influence on magma supply at the East Scotia Ridge. Earth Planet. Sci. Lett. 1997 (150), 261–275.

Loreto, M.F., Zitellini, N., Ranero, C., Palmiotto, C., Manel, P., 2020. Extensional tectonics during the Tyrrhenian back-arc basin formation and a new morphotectonic map. Basin Res. 33, 138–158.

Lupton, J., De Ronde, C., Sprovieri, M., Baker, E.T., Bruno, P.P., Italiano, F., Walker, S., Faure, K., Leybourne, M., Britten, K., Greene, R., 2011. Active hydrothermal discharge on the submarine Aeolian Arc. J. Geophys. Res. 116, 1–22.

Macdonald, K.C., Fox, P.J., Perram, L.J., Eisen, M.F., Haymon, R.M., Miller, S.P., Carbotte, S.M., Cormier, M.H., Shor, A.N., 1988. A new view of the mid-ocean ridge from the behaviour of ridge-axis discontinuities. Nature 335, 217–225.

Mackenzie, F.T., Andersson, A.J., 2013. The marine carbon system and ocean acidification during Phanerozoic time. Geochem. Perspect. 2 (1), 1–227.

Magni, V., Naliboff, J., Prada, M., Gaina, C., 2021. Ridge Jumps and Mantle Exhumation in Back-Arc Basins. Geosciences 11, 475.

Malinverno, A., Ryan, W.B., 1986. Extension in the Tyrrhenian Sea and shortening in the Apennines as result of arc migration driven by sinking of the lithosphere. Tectonics 5 (2), 227–245.

Marani, M., Gamberi, F., 2004. Structural framework of the Tyrrhenian Sea unveiled by seafloor morphology. Mem. Descr. Carta Geol. d'It. 44, 97–108.

Marani, M., Bonatti, E., Gamberi, F., 2004. From seafloor to deep mantle: architecture of the Tyrrhenian back-arc basin. Mem. Descr. Carta Geol. D'It. 64, 1–194.

Marani, M., Trua, T., 2002. Thermal constriction and slab tearing at the origin of a superinflated spreading ridge: Marsili volcano (Tyrrhenian Sea). J. Geophys. Res. 107 https://doi.org/10.1029/2001JB000285.

Martinez, F., Taylor, B., 2002. Mantle wedge control on back-arc crustal accretion. Nature 416, 417–420.

McKenzie, F.T., Bernoulli, D., 1982. Geochemical variations in Quaternary hardgrounds from trhe Hellenic trench region and possible relationship to their tectonic setting. Tectonophysics 86, 149–157.

Morse, J.W., 1986. The surface chemistry of calcium carbonate minerals in natural waters: an overview. Mar. Chem. 20, 91–112.

Morse, J.W., McKenzie, F.T., 1990. Geochemistry of sedimentary carbonates. Dev. Sedimentol. 48, 696.

Mutti, M., Bernoulli, D., 2003. Early marine lithificaion and hardground development on a Miocene ramp (Maiella, Italy) key surfaces to rack changes in trophic resources in nontropical carbonate settings. J. Sediment. Res. 73, 296–308.

Nicolosi, I., Speranza, F., Chiappini, M., 2006. Ultrafast oceanic spreading of the Marsili Basin, southern Tyrrhenian Sea: Evidence from magnetic anomaly analysis. Geology 34. https://doi.org/10.1130/G22555.1.

Pagli, C., Sang-Ho, Y., Ebinger, C., Keir, D., Wang, H., 2019. Strike-slip tectonics during rift linkage. Geology 47, 31–34.

Palmiotto, C., Loreto, M.F., 2019. Regional scale morphological pattern of the Tyrrhenian Sea: New insights from EMODnet bathymetry. Geomorphology 332, 88–99.

Palmiotto, C., Ficini, E., Loreto, M.F., Muccini, F., Cuffaro, M., 2022. Back-Arc Spreading Centers and Superfast Subduction: the Case of the Northern Lau Basin (SW Pacific

Ocean). Geosciences 12, 50.

Parson, L.M., Wright, I.C., 1996. The Lau-Havre-Taupo back-arc basin: a southwardpropagating, multi-stage evolution from rifting to spreading. Tectonophysics 263, 1–22.

Parson, L.M., Pearce, J.A., Murton, B.J., Hodkinson, R.A., the RRS Charles Darwin Scientific Party, 1990. Role of ridge jumps and ridge propagation in the tectonic evolution of the Lau back-arc basin, Southwest Pacific. Geology 18, 470–473.

Pearce, J., Cann, J., 1973. Tectonic setting of Basic Volcanic Rocks determined using Trace Element analyses. Earth Planet. Sci. Lett. 19, 290–300.

Pearce, J.A., 2014. Immobile Element Fingerprinting of Ophiolites. Elements 10, 101–108.

Peccerillo, A., 2005. Plio-Quaternary Volcanism in Italy, vol. 365. Springer Verlag, Berlin Heidelberg.

Peccerillo, A., 2017. Southern Tyrrhenian Sea. Cenozoic volcanism in the Tyrrhenian Sea region, advances in volcanology. Springer, pp. 339–362.

Pensa, A., Pinton, A., Vita, L., Bonamico, A., De Benedetti, A.A., Giordano, G., 2019. ATLAS of Italian submarine volcanic structures. Mem. Descr. Carta Geol. d'It. 104, 77–183.

Prada, M., Sallares, V., Ranero, C.R., Vendrell, M.G., Grevemeyer, I., Zitellini, N., De Franco, R., 2014. Seismic structure of the Central Tyrrhenian basin: Geophysical constraints on the nature of the main crustal domains. J. Geophys. Res. Solid Earth 119 (1), 52–70.

Prada, M., Ranero, C.R., Sallar`es, V., Zitellini, N., Grevemeyer, I., 2016. Mantle exhumation and sequence of magmatic events in the Magnaghi-Vavilov Basin (Central Tyrrhenian, Italy): New constraints from geological and geophysical observations. Tectonophysics 689, 133–142.

Prada, M., Sallares, V., Ranero, C.R., Vendrell, M.G., Grevemeyer, I., Zitellini, N., De

Franco, R., 2018. Spatial variations of magmatic crustal accretion during the opening of the Tyrrhenian back-arc from wide-angle seismic velocity models and seismic reflection images. Basin Res. 30, 124–141.

Ranero, C.R., Sallar´es, V., Zitellini, N., Grevemeyer, I., Guzman, M., Prada, M., Moeller, S., De Franco, R., Party, The Medoc Cruise, 2012. The tectonic structure of the Tyrrhenian Basin, a complex interaction among faulting and magmatism. Rend. Online Soc. Geol. It. 21, 251–252.

Recq, M., Rehault, J.P., Steinmetz, L., Fabbri, A., 1984. Amincissement de la croute et accretion au centre du bassin Tyrrhenien d'apres la sismique refraction. Mar. Geol. 55, 411–428.

Rehault, J.P., Moussat, E., Fabbri, A., 1987. Structural evolution of the Tyrrhenian backarc basin. Mar. Geol. 74 (1–2), 123–150.

Remia, A., Montagna, P., Taviani, M., 2004. Submarine diagenetic products on the sediment-starved Gorgona slope, Tuscan Archipelago (Tyrrhenian Sea). Chem. Ecol. 20 (1), 131–153.

Robin, C., Colantoni, P., Gennesseaux, M., Reehault, J.P., 1987. Vavilov seamount: a mild alkaline Quaternary volcano in the Tyrrhenian basin. Mar. Geol. 78, 125–136.

Rosenbaum, G., Gasparon, M., Lucente, F.P., Peccerillo, A., Miller, M.S., 2008. Kinematics of slab tear faults during subduction segmentation and implications for Italian magmatism. Tectonics 27 (2).

Rovere, M., Wurtz, M., 2015. Atlas of the Mediterranean Seamounts and Seamount-like Structures. IUCN, Gland, Switzerland and Malaga, Spain.

Sartori, R., 1986. Notes on the geology of the acoustic basement in the Tyrrhenian Sea. Mem. Soc. Geol. It. 36, 99–108.

Sartori, R., 2003. The Tyrrhenian back-arc basin and subduction of the Ionian lithosphere. Episodes 26 (3), 217–221.

Savelli, C., 1988. Late Oligocene to recent episodes of magmatism in and around the Tyrrhenian Sea: implications for the processes of opening in a young inter-arc basin of intra-orogenic (Mediterranean) type. Tectonophysics 146, 163–181.

Savelli, C., Ligi, M., 2017. An updated reconstruction of basaltic crust emplacement in Tyrrhenian Sea, Italy. Sci. Rep. 7 (1), 1–12.

Schellart, W.P., Freeman, J., Stegman, D.R., Moresi, L., May, D., 2007. Evolution and diversity of subduction zones controlled by slab width. Nat. Lett. 446, 308–311.

Schliffke, N., Van Hunen, J., Allen, M.B., Magni, V., Gueydan, F., 2022. Episodic back-arc spreading Centre jumps controlled by transform fault to overriding plate strength ratio. Nat. Commun. 13, 582.

Scrocca, D., Doglioni, C., Innocenti, F., Manetti, P., D'Offizi, S., 2003. CROP Atlas: seismic reflection profiles of the Italian crust. Mem. Descrit. Carta Geolo. d'It. 62, 1–193.

Sdrolias, M., Muller, R.D., 2006. Controls on back-arc basin formation. Geochem. Geophys. Geosyst. 7 (4), 1–40.

Selli, R., Lucchini, F., Rossi, P.L., Savelli, C., Del Monte, M., 1977. Dati geologici, petrochimici e radiometrici sui vulcani centro-tirrenici. Giorn. Geol. 42, 221–246.

Serri, G., Innocenti, F., Manetti, P., 2001. Magmatism from Mesozoic to present: Petrogenesis, time-space distribution and geodynamic implications. In: Vai, G.B., Martini, P.I. (Eds.), Anatomy of a Mountain: The Appenines and the Adjacent Mediterranean Basins, Dordrecht, the Netherland. Kluwer Academic Publishers, pp. 77–104.

Trincardi, F., Zitellini, N., 1987. The rifting of the Tyrrhenian Basin. Geo-Mar. Lett. 7 (1), 1–6.

Trua, T., Serri, G., Marani, M., Renzulli, A., Gamberi, F., 2002. Volcanological and petrological evolution of Marsili Seamount (southern Tyrrhenian Sea). J. Volcanol. Geotherm. Res. 114 (3–4), 441–464.

Trua, T., Serri, G., Rossi, P.L., 2004. Coexistence of IAB-type and OIB-type magmas in the southern Tyrrhenian back-arc basin: evidence from recent seafloor sampling and geodynamic implications. Mem. Descrit. Carta Geolo. d'It. 44, 83–96.

Trua, T., Marani, M., Gamberi, F., 2018. Magma plumbing system at a Young Back-Arc spreading center: The Marsili volcano, Southern Tyrrhenian Sea. Geochem. Geophys. Geosyst. 19.

Uyeda, S., Kanamori, H., 1979. Back-arc opening and the mode of subduction. J. Geophys. Res. 84, 1049–1061.

Van Van Dijk, J.P., Bello, M., Brancaleoni, G.P., Toscano, C., 2000. A regional structural model for the northern sector of the Calabrian Arc (southern Italy). Tectonophysics 324 (4), 267–320.

Ventura, G., Milano, G., Passaro, S., Sprovieri, M., 2013. The Marsili Ridge (Southern Tyrrhenian Sea, Italy): an island-arc volcanic complex emplaced on a 'relict' backarc basin. Earth Sci. Rev. 116, 85–94.

Weins, D.A., Kelley, K.A., Plank, T., 2006. Mantle temperature variations beneath backarc spreading centers inferred from seismology, petrology, and bathymetry. Earth Planet. Sci. Lett. 248, 30–42.

Wessel, P., Smith, W.H.F., 1998. New improved version of the generic mapping tools released. EOS Trans. Am. Geophys. Union 79, 579.

Wezel, F.C., 1982. The Tyrrhenian Sea: a rifted Krikogenic-Swell Basin. Mem. Soc. Geol. It. 24, 531–568.

Wilkinson, M.D., Dumontier, M., Aalbersberg, I.J., Appleton, G., 2016. The FAIR guiding principles for scientific data management and stewardship. Scientific Data 3, 160018.

Zankl, H., 1969. Structural and Textural evidence of early lithification in fine grained carbonate rocks. Sedimentology 12, 241–256.

Zitellini, N., Trincardi, F., Marani, M., Fabbri, A., 1986. Neogenic tectonic of the Northern

Tyrrhenian Sea. Giorn. Geol. 48, 25–40.

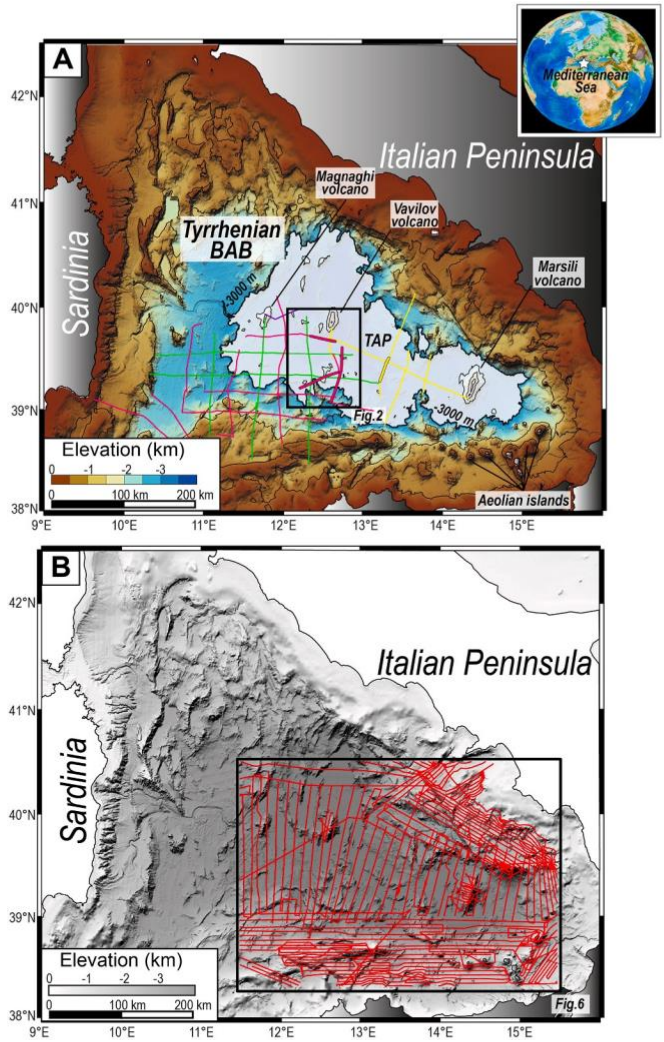

Fig. 1. Geographic setting of the Mediterranean Sea (white star). A) Base colored bathymetry map of the Tyrrhenian Back-Arc Basin (BAB). Black square is the area shown in Fig. 2; black lines are isobaths (interval of 1000 m); the Tyrrhenian Abyssal Plain (TAP), deeper than 3000 m, has been evidenced with the white area; yellow, green and pink lines are the location of sparker lines acquired in the 1971, 1973 and 1975, respectively. Thicked lines indicate parts of the seismic profiles interpreted in this paper. B) Base shaded bathymetry map of the Tyrrhenian BAB. Black square is the area shown in Fig. 6; black line is the coast line; red lines are the location of the magnetic lines acquired in the 1996 and 1999. Bathymetry has been downloaded EMODnet portal (http://portal. emodnet-bathymetry.eu/gebco-bathymetry-basemap) and gridded using GMT open software; bathymetric data have been used to create 2D digital elevation model image using Global Mapper Software.

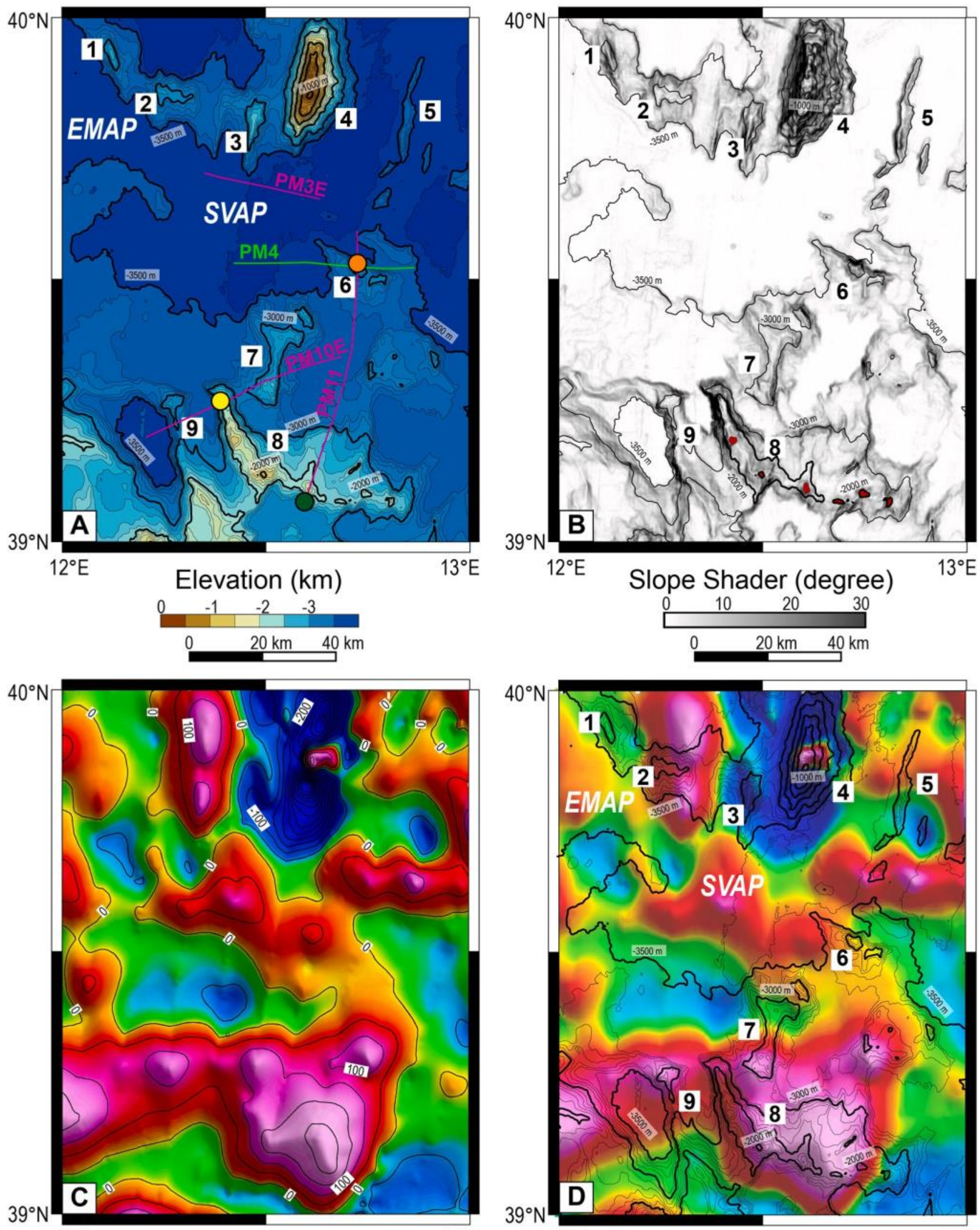

Fig. 2. Maps of the bathymetry and of the reduced to the pole magnetic anomalies of the Southern Vavilov region. A) Shaded relief image of the bathymetry. Sun angle: 70◦; Azimuth: 330◦. Vertical Exaggeration: 10. Contour black lines are isobaths every 100 m; green and pink lines indicate the location of the sparker lines shown in Fig. 3; orange, yellow and green dots are the points of the dredges (75–30, 75–35 and 75–36, respectively). B) Slope shader relief map of the bathymetry (isobath interval of 500 m). Red areas show the six peaks along the summit of the Augusto Seamount. Sun angle: 70◦; Azimuth: 330◦. Vertical Exaggeration: 10. C) Shaded relief image of the distribution of the reduced to the pole magnetic anomalies where contour black lines indicate the lines with the same anomaly value (interval of 50 nT). D) Shaded relief image of the distribution of the reduced to the pole magnetic anomalies where contour black lines are isobaths (interval of 100 m). 1. D'Ancona I Seamount; 2. D'Ancona II Seamount; 3. Plinia Seamount; 4. Vavilov Seamount; 5. Tibullo Seamount; 6. Aurelia Seamount; 7. Virgilio Seamount; 8. Augusto Seamount; 9. Emilia Seamount.

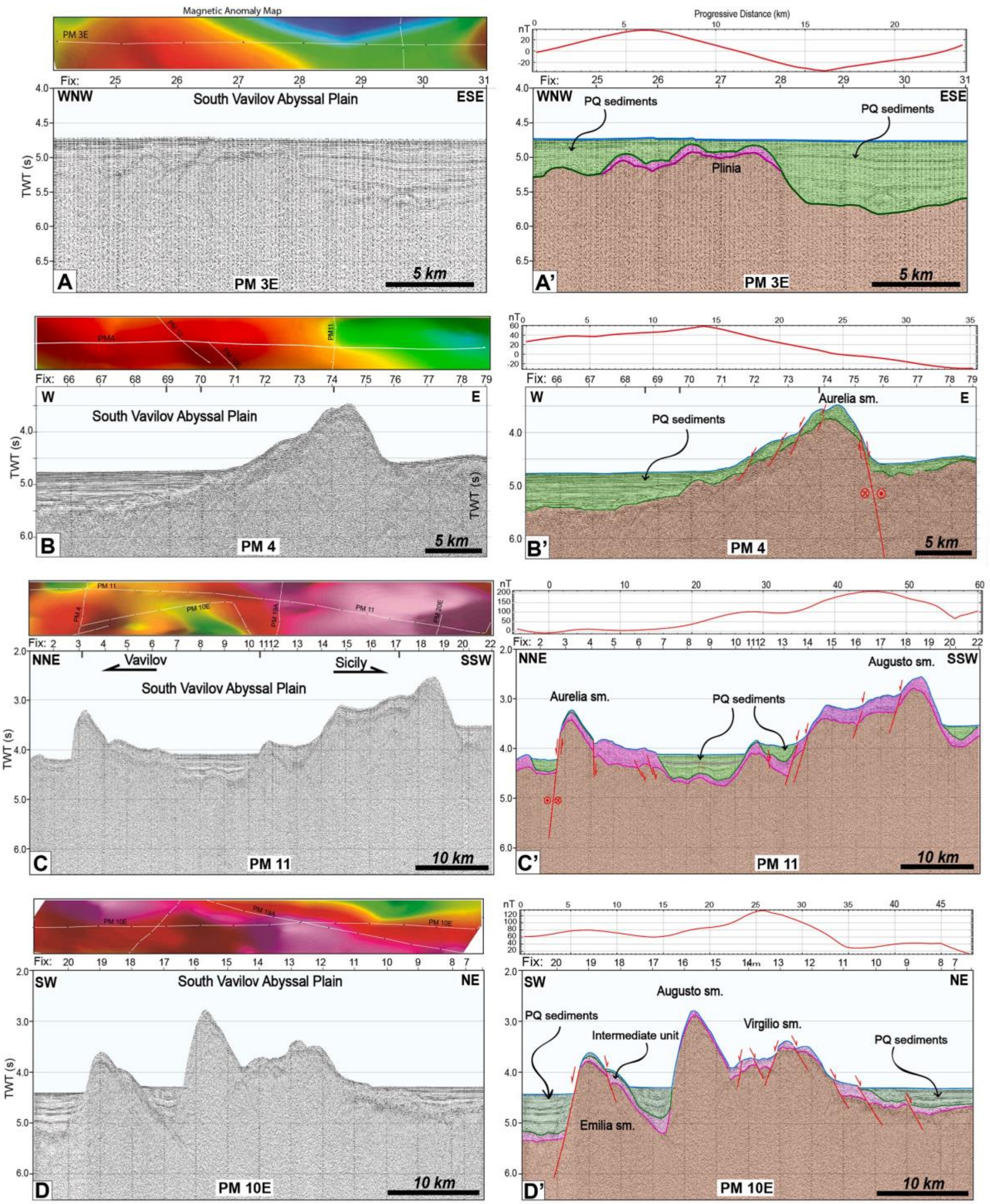

Fig. 3. Sparker profiles with their relative interpretation, maps of magnetic anomaly and magnetic profiles extracted along the profiles. (A-A') Sparker Line PM3E; (B-B') Sparker Line PM4; (C-C') Sparker Line PM11; (D-D') Sparker Line PM10E

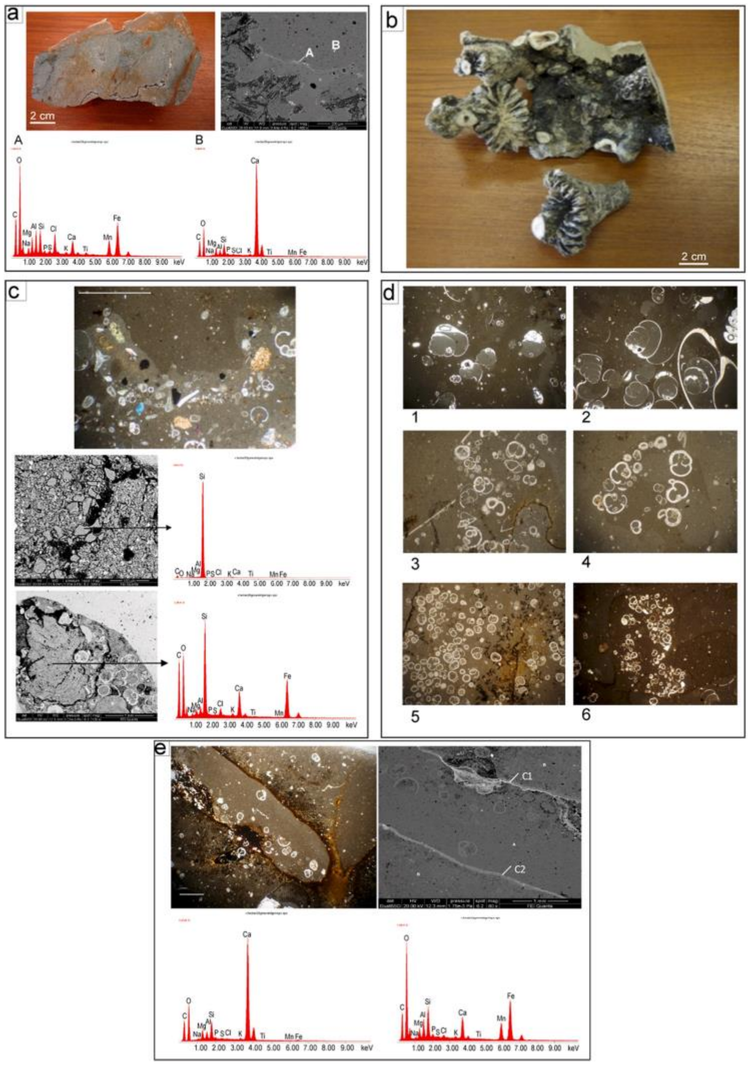

Fig. 4. (a) Sample from dredge 75–30-3 (Aurelia Seamount). Macroscopic view of the direct contact between the volcanic substrate and the overlying carbonate crust. Neptunian dykes filled by carbonate mud are also visible; SEM photomicrograph of the sample: the related EDAS spectrum B evidenced a predominantly carbonate composition of the crust with a very subordinate clay-sized silicate fraction; the black film marking the contact with the volcanic substrate is represented by Mn−Fe oxides (spectrum A). (b) Black-coated corals (*Desmophyllum*) from dredge 75–35-5 (western Augusto Seamount), scale bar 2 cm. (c) Thin section photomicrographs from dredge 75–36-7A sample (eastern Augusto Seamount) showing isolated volcanic minerals scattered within the planktonic-rich carbonate mud; quartz grains are also evidenced by the SEM photomicrograph of the sample and the related EDAS spectrum. (d) Thin section photomicrographs of the carbonate crusts: 1–2) geopetal structures in pteriopod-foraminifer wackestone, pteropod sections are partially filled by foraminifer micrite and microspar at the top; 3) planktonic foraminifera: *Pulleniatina obliquiloculata*, globigerinids, *Globorotalia truncatulinoides* (dredge 75–30-3 sample), scale bar 500 µm; 4) planktonic foraminifera: *Pulleniatina obliquiloculata*, globigerinids (dredge 75–30-3 sample), scale bar 500 µm; 5) planktonic foraminifera: *Pulleniatina obliquiloculata*, globigerinids, *Globorotalia inflata*, *Globigerinoides* spp. (dredge 75–36-7A sample), scale bar 1 mm; 6) cloud of planktonic foraminifera, pteropods shell, bioturbation evidences (dredge 75–36-7A sample), scale bar 1 mm. (e) Sample from dredge 75–36-7A. Thin section photomicrograph showing a boring structure filled by planktonic-foraminifer mud; SEM photomicrograph of the sample and the related EDAS spectra evidencing the same composition of the carbonate mud outside and inside the cavity (A and B spectra) and the Mn−Fe oxides-rich film coating the boring.

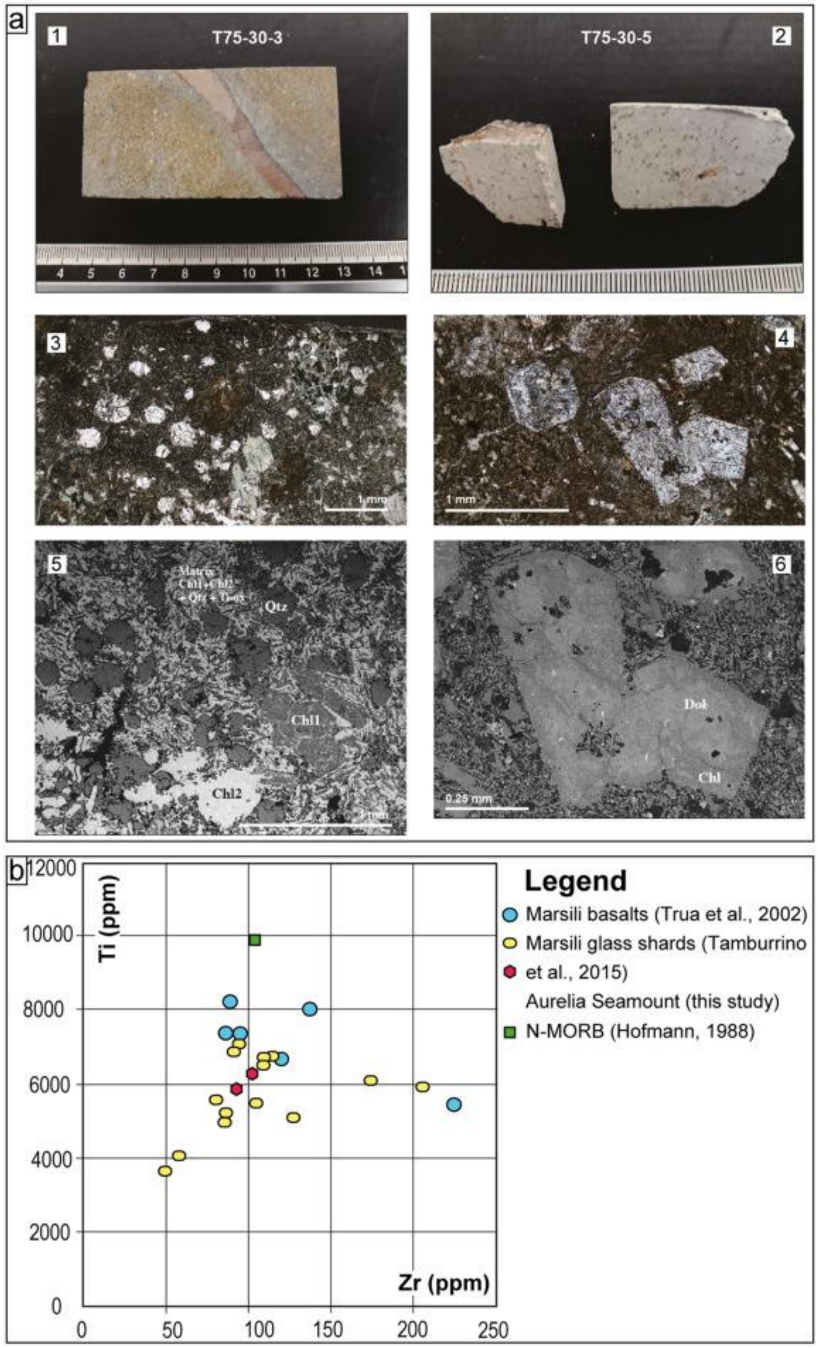

Fig. 5. (a) 1–2) Low-magnification overview of the chosen samples. (3–4) Photomicrographs (plane polarized light) showing altered phenocryst with euhedral to subhedral shape. (5–6) Backscattered electron images with phase labelling based on EDS microanalysis. Early igneous phenocrysts are now replaced by secondary phases, mostly chlorite and dolomite. (b) Ti–Zr discrimination diagram (Cann, 1970; Pearce and Cann, 1973) where the data of this study are compared to available data from the Marsili Volcano (Pearce, 2014).

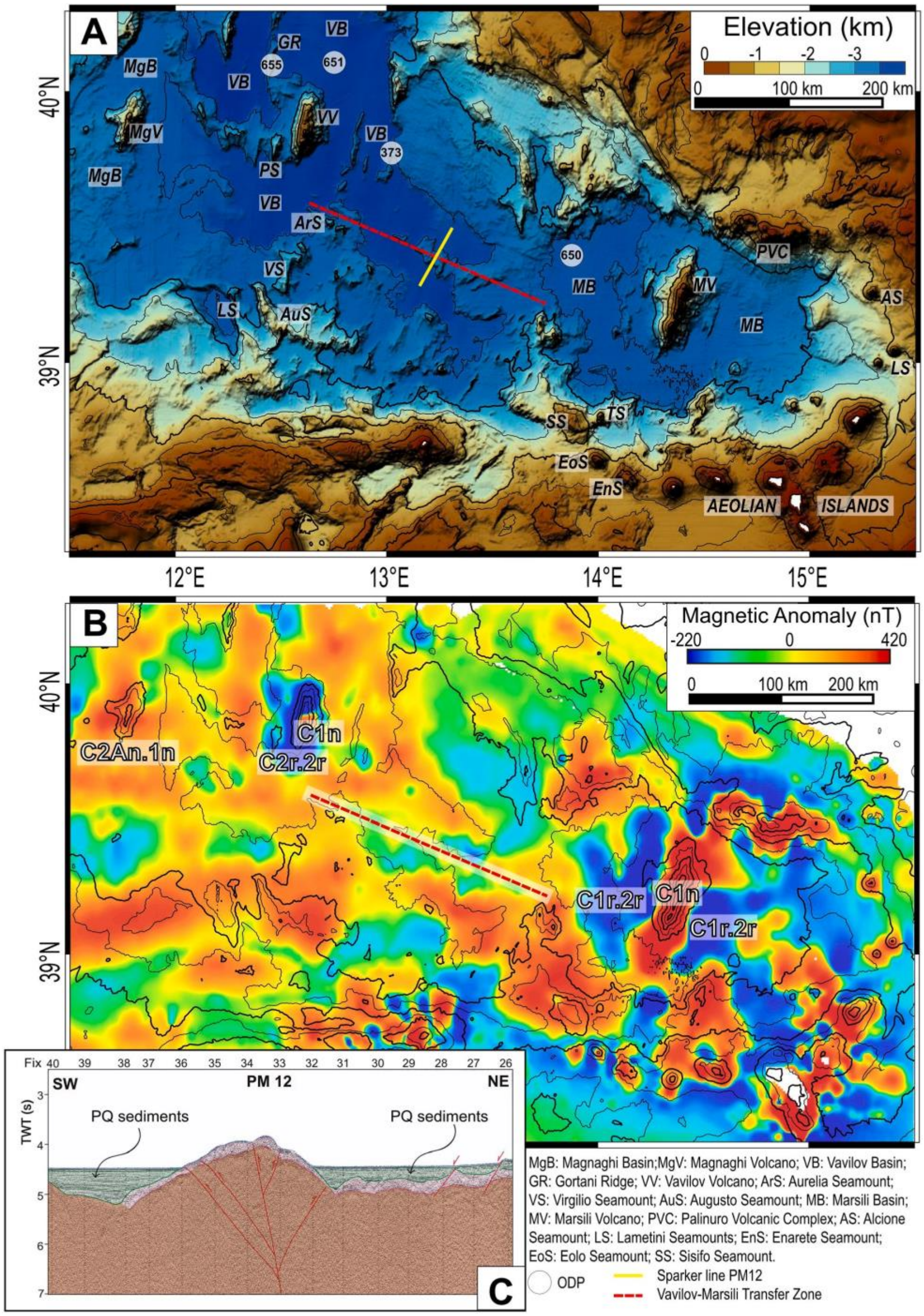

Fig. 6. A) Shaded relief bathymetric image of the Southern Tyrrhenian Sea. Bathymetry has been downloaded EMODnet portal (http://portal.emodnet-bathymetry. eu/gebco-bathymetry-basemap) and gridded using GMT open software; bathymetric data have been used to create 2D digital elevation model image using Global Mapper Software. Sun angle: 70◦; Azimuth: 330◦. Vertical Exaggeration: 10. B) Map of the distribution of the reduced to the pole magnetic anomalies in the Southern Tyrrhenian Sea. Black contour lines are isobaths every 500 m. C) Sparker Profile PM12 with interpretation.

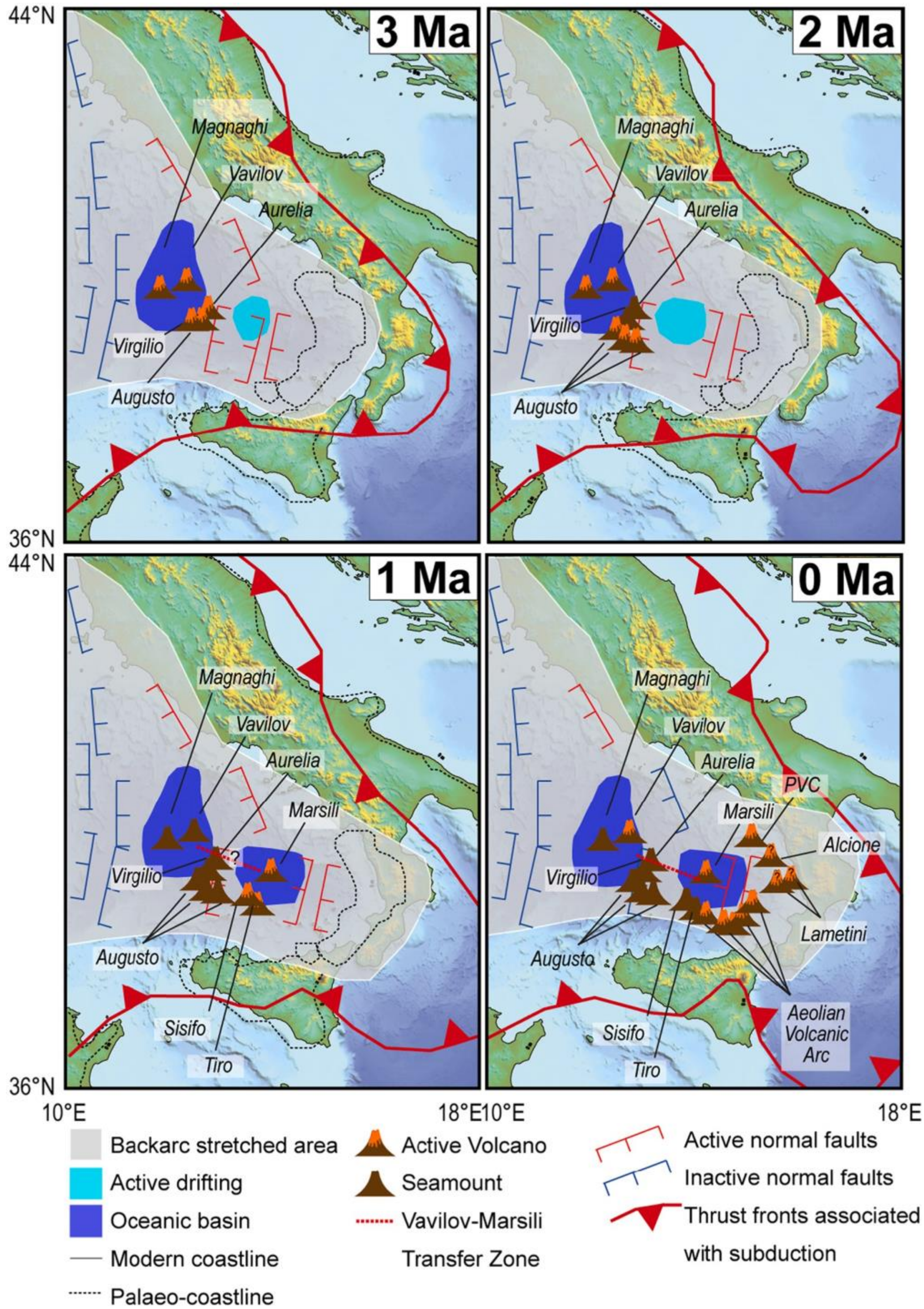

Fig. 7. Cartoon showing the formation and evolution of the volcanic arc related to the Ioanian subduction during the last 3 Ma. Geodynamic reconstruction is based on the model published by Carminati et al. (2010). 3 Ma) Active volcanism of the Magnaghi and Vavilov volcanoes; the active arc is formed by the Aurelia, the Virgilio and the Western part of the Augusto Seamount. 2 Ma) Active volcanism of the Magnaghi and Vavilov volcanoes; the active arc is formed by the Augusto Seamount. 1 Ma) Active volcanism of the Marsili volcano; the active arc is formed by the Sisifo and Tiro Seamounts. 0 Ma) Active volcanism of the Vavilov and Marsili volcanoes; the active arc is formed by the Aeolian Islands and Seamounts.